aerospace

MDPI

Communication

Experimental Investigation of Cavity Flame Characteristics for Variable-Angle Dual Injection in a Ma = 1.6 Supersonic Combustor

Lantian Li and Jianhan Liang *

National Key Laboratory of Advanced Propulsion Technology, National University of Defense Technology, Changsha 410073, China; lilantian1994@126.com
* Correspondence: jhleon@vip.sina.com

Abstract

Robust flame stabilization in low-Mach, low-enthalpy supersonic combustors is a core bottleneck for turbine-based combined cycle (TBCC) mode transition. Existing studies mainly focus on single-injector configurations, while the injection angle modulation mechanism for multi-injector cavity flameholders remains unclear under TBCC-relevant conditions. This work experimentally investigated the effects of 30°, 45°, and 90° injection angles on cold-flow mixing, reacting flow topology, and flame stabilization in a Mach 1.6, 660 K dual-injector cavity combustor. Results showed that the overall cold-flow jet penetration capacity in the fully developed far field increased with injection angle following the order of 90° > 45° > 30°. Combustion heat release universally enhanced jet penetration, with a maximum 25% augmentation observed at 30° injection, which attenuated with steepening injection angle. Moreover, flame stability exhibited a non-monotonic trend in the tested dual-injector configuration.

Keywords: cavity-stabilized combustor; dual injection; injection angle; flame stability; supersonic flow; low-enthalpy combustion

1. Introduction

Cavity flameholding is the dominant strategy for reliable ignition and sustained combustion in low-Mach, low-enthalpy scramjet engines, especially for TBCC mode transition at Mach 1.2–2.0 [1–5], where narrow ignition margin and poor flame stability restrict engine operability.

Fuel injection angle directly modulates jet penetration depth, shock structure, shear layer dynamics, and fuel–air mixing, thus dominating combustor performance.

In single-injector cavity combustors, the injection angle is a primary parameter controlling jet penetration and flame stabilization. Early experiments by Gruber et al. [6]. and the correlation developed by Portz and Segal [7] established that jet penetration depth increases monotonically with the effective transverse momentum flux in supersonic crossflows. Further studies on cavity flameholders [8,9] consistently demonstrated that larger injection angles enhance fuel entrainment into the recirculation zone and thus improve flame stability, forming a well-accepted monotonic positive correlation. This relationship has been quantitatively verified by PLIF measurements [10] and numerically extended to broader angle ranges, where competing effects on pressure loss and mixing efficiency emerge at low injection angles [11]. To date, systematic experimental quantification of injection angle effects on cavity combustors with a dual-orifice injection configuration under TBCC-relevant

Check for updates

Academic Editor: James 'Chris' Thomas

Received: 28 April 2026
Revised: 18 June 2026
Accepted: 25 June 2026
Published: 26 June 2026

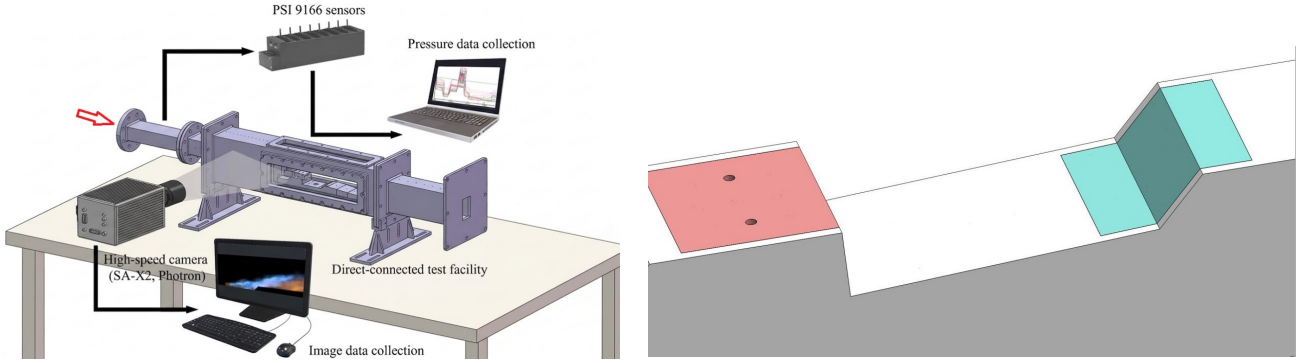
Copyright: © 2026 by the authors. Licensee MDPI, Basel, Switzerland. This article is an open access article distributed under the terms and conditions of the Creative Commons Attribution (CC BY) license.

low-Mach, low-enthalpy conditions remains absent, and the underlying mechanism of injection angle modulation on flame stabilization has not been clearly clarified [9]. Here, we characterize 30°, 45°, 90° injection effects on a Mach 1.6 dual-injector cavity combustor via high-speed schlieren and CH* chemiluminescence. The core contribution of this work is the systematic experimental characterization of angle-dependent combustion-induced penetration augmentation and the non-monotonic flame stability law in a dual-orifice cavity configuration, with the governing mechanism attributed to the coupling between flame front and cavity shear layer.

2. Experimental Setup

2.1. Experimental and Injection Configuration

The overall experimental configuration was shown in Figure 1a. All the tests were carried out in a direct-connected supersonic combustion test facility, which is well validated in previous supersonic combustion studies [12], and provided uniform, steady, and repeatable supersonic inflow.



(**a**) (**b**)

Figure 1. Schematic of the experimental setup. (**a**) Overall schematic of the supersonic combustion test system. (**b**) Schematic of the dual-orifice injection configuration upstream of the cavity leading edge. The orifices are symmetrically placed 20 mm from the cavity leading edge.

The combustor has a rectangular inlet with the cross-section of 50 mm × 30 mm, and It was extended to a 250 mm duct with a half expansion angle of 3.43° to avoid thermal choking. A 90 mm long rectangular cavity flameholder was mounted on the lower wall, with its position defined relative to the combustor inlet; for the sake of clarity in the following analysis, the streamwise coordinate x was taken from the cavity leading-edge inflection point, and the distances were normalized by the cavity floor length $L_{bottom} = 78.8$ mm for the comparison of different configuration schemes. The cavity has an upper length-to-depth ratio $L_{upper}/D = 5$ ($L_{upper} = 90$ mm, $D = 18$ mm), a right-angle leading edge and 45° beveled trailing edge.

The nominal inflow conditions were set at $Ma = 1.6$, $T_0 = 660$ K, $P_0 = 0.4$ Mpa, and a mass flux of 0.735 kg/s, and the flow uncertainty measured was less than 1%.

The dual-orifice fuel injection configuration is shown in Figure 1b. Gaseous ethylene was injected through two symmetric circular orifices, located 20 mm upstream of the cavity leading edge, with a total orifice area of 12.57 mm^2, and an orifice spacing of 16.67 mm. Dedicated fuel mass flow rate compensation was performed during the adjustment of the injection angle to eliminate the influence of angle variation on fuel supply state and combustion boundary conditions. The fuel mass flow rate was adjusted for different injection angles to have the same fuel supply conditions. Fuel was injected at the gauge pressure of 1 MPa and ambient temperature of 300 K with the fixed global equivalence

ratio $\phi = 0.2$, which is a typical stable operating point for low-Mach cavity-stabilized supersonic combustion. The injection parameters were summarized in Table 1. The fuel mass flow rate was controlled with an uncertainty of 1% or less. All the tests were repeated at least three times to be sure about the experimental repeatability.

Table 1. Key parameters of the fuel injection configurations.

Injection Angle	Jet Orifice Diameter (mm)	Global Equivalence Ratio	Momentum Flux Ratio J	Normal Momentum Ratio $J \cdot \sin^2\theta$
30°	2.83	0.2	2.24	0.56
45°	2.83	0.2	2.24	1.12
90°	2.83	0.2	2.24	2.24

2.2. Measurement and Data Processing

For flow field and flame measurements, two synchronized optical diagnostic systems, a Z-type schlieren system and a side-view CH* chemiluminescence system, were used. The schlieren system was equipped with a 500 W xenon lamp and was operated at 10,000 frames per second (fps) with a shutter speed of 1/990,000 s. For flame emission, the CH* system used 430 ± 10 nm bandpass filter and was operated at 10,000 fps with shutter speed = 1/10,000 s. Both systems were coupled to a Photron FASTCAM SA-X2 high-speed camera (1024 × 1024 pixel resolution), and synchronization accuracy is ±1 μs. Time averaged and root-mean-square (RMS) fluctuation field were calculated from the CH* chemiluminescence image sequences [13].

The jet penetration depth was extracted from the time-averaged schlieren images with a multi-scale gray-level step detection algorithm. For every column in the masked flow region, the jet boundary was taken as the pixel where the absolute difference in the local mean intensities above and below was the maximum, which was the steepest density gradient. A Hough-transform-based shock mask was used to suppress spurious responses close to the shock wave. The detected boundary points were filtered by interactive outlier removal and by manual supplementation. They were then smoothed with a robust Savitzky–Golay filter to obtain a continuous penetration profile [14].

3. Results and Discussion

3.1. Cold-Flow Characteristics

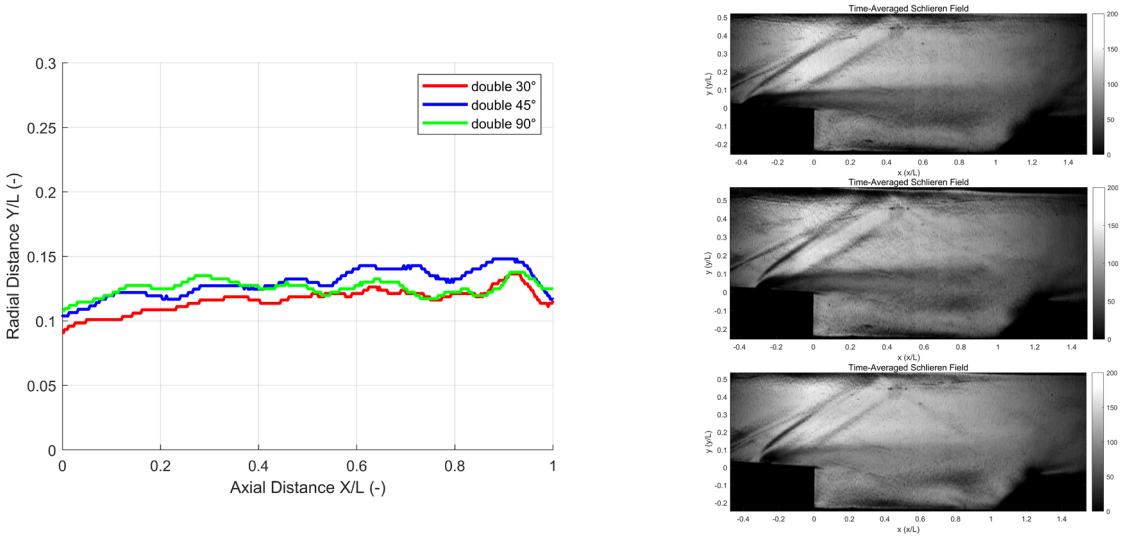
We carried cold-flow experiments at $Ma = 1.6$, $T_0 = 660$ K, and global equivalence ratio $\phi = 0.2$. The influence of injection angle (30°, 45°, and 90°) on the jet trajectory, shock structure, and the behavior of cavity flow in the dual-injector configuration is characterized by using the axially normalized fuel jet penetration depth profiles (Figure 2a) and the time-averaged schlieren visualizations (Figure 2b).

3.1.1. Jet Penetration Depth and Its Variation with Injection Angle

The quantitative analysis showed that there were two different axial regimes of the jet penetration depth, which are common to all the injection angles and have high temporal repeatability:

Initial penetration regime ($x/L = 0$–0.2)

The near-field behavior was affected by both the jet transverse momentum and the cavity shear layer; the crossflow entrainment and deceleration had not yet been established. Therefore, the penetration depth increased almost linearly with the axial distance, and followed the order of 30° > 45° > 90° in this region due to the stronger lifting effect of the cavity shear layer on small-angle jets.



(**a**) (**b**)

Figure 2. Jet penetration depth characteristics and schlieren flow field structure in supersonic cold-flow conditions: (**a**) the curve of cold-flow jet penetration depth which is normalized by L_{bottom} = 78.8 mm; (**b**) time-averaged cold-flow schlieren flow fields at injection angles of 30°, 45° and 90° are arranged from top to bottom, demonstrating jet-induced shock structures and cavity shear layer characteristics.

Quasi-steady regime (x/L = 0.2–1.0)

The momentum exchange between the jet and crossflow became dynamic balance, and the penetration depth reached a plateau with small-amplitude oscillation. In the far field of this regime, the penetration depth scaled monotonically with the transverse momentum flux, following the order of 90° > 45° > 30°. This trend was consistent with the single-injector results reported in Refs. [6,8]: a larger injection angle corresponded to a higher transverse momentum flux imparted to the jet, which enabled deeper penetration of the jet into the supersonic core flow. The temporal fluctuation amplitude is less than 0.02 y/L for all cases, which meant that the cold-flow unsteadiness is negligible compared with the combustion-driven variation in the following reacting tests.

As the jet developed downstream, gradual jet–crossflow mixing blurred the density gradient at the jet upper boundary and reduced the measurement accuracy of schlieren-based penetration extraction. Thus, the results in this downstream regime only served as a quasi-quantitative trend comparison. Specifically, in the region where x/L > 0.4, the increasing trend of penetration depth for the 90° injection case diminished significantly. The core mechanism is that the 90° injection induced stronger shear and faster fuel–air mixing in the upstream section, which attenuated the jet boundary contrast more rapidly, making the effective penetration front indistinct in the downstream flow field.

3.1.2. Flow Structure and Shock Wave Features Under Different Injection Schemes

Injection angle also strongly influenced the strength, structure, and location of the jet-generated shocks, as can be seen in the schlieren visualizations, which in turn determined the combustor total pressure loss [4,15].

The injection 30° downstream introduced a little disturbance to the oncoming flow, and only a weak oblique shock was produced downstream of the orifice. It had the lowest density gradients and therefore the smallest total pressure loss.

The 90° normal injection caused the most severe flow blockage to the crossflow, forming a well-defined bow shock upstream of the injector. The strong density jump across

this shock led to the highest total pressure loss among the three cases; yet, it achieved a significantly faster fuel–air mixing rate than the other configurations.

The 45° injection had also intermediate shock strength and pressure loss, and followed almost a linear behavior with the injection angle in the range tested.

These results are in agreement with the well-known trade-off between jet penetration depth and total pressure loss in supersonic combustors, and it confirmed that the injection angle is another parameter that can be used to balance the combustor performance and the pressure recovery.

3.1.3. Jet Interaction with Cavity Shear Layer

The injection angle modulated the cavity shear layer impingement height and recirculation zone extent—key factors governing flame stabilization—via its effect on jet penetration depth. In the dual-injector configuration, jet–jet interactions further modulate the jet–shear layer coupling behavior.

The 30° injection: The jet exhibited strong interaction with the cavity shear layer. On one hand, a large portion of the jet penetrated into the cavity through the wake flow; on the other hand, intense coupling between the jet and the shear layer was dominated by the counter-rotating vortex pair (CVP) based on inference from established JICF theory.

The 90° injection: The jet achieved a higher penetration depth and exhibited weaker interaction with the cavity shear layer.

The 45° injection: The configuration yielded intermediate jet penetration depth, with a moderate level of jet–shear layer interaction intensity (weaker than the 30° injection case).

3.2. Reacting Flow Characteristics

In this section, the reacting flow behavior at injection angles of 30°, 45° and 90° was characterized for the same baseline ($Ma = 1.6$, $T_0 = 660$ K, $\phi = 0.2$). Figure 3a gave the normalized fuel jet penetration depth in reacting flow, and Figure 3b showed the time-averaged schlieren visualizations. By comparing directly with the cold-flow data (Section 3.1), we can quantify how the combustion heat release modulated the overall flow field topology.

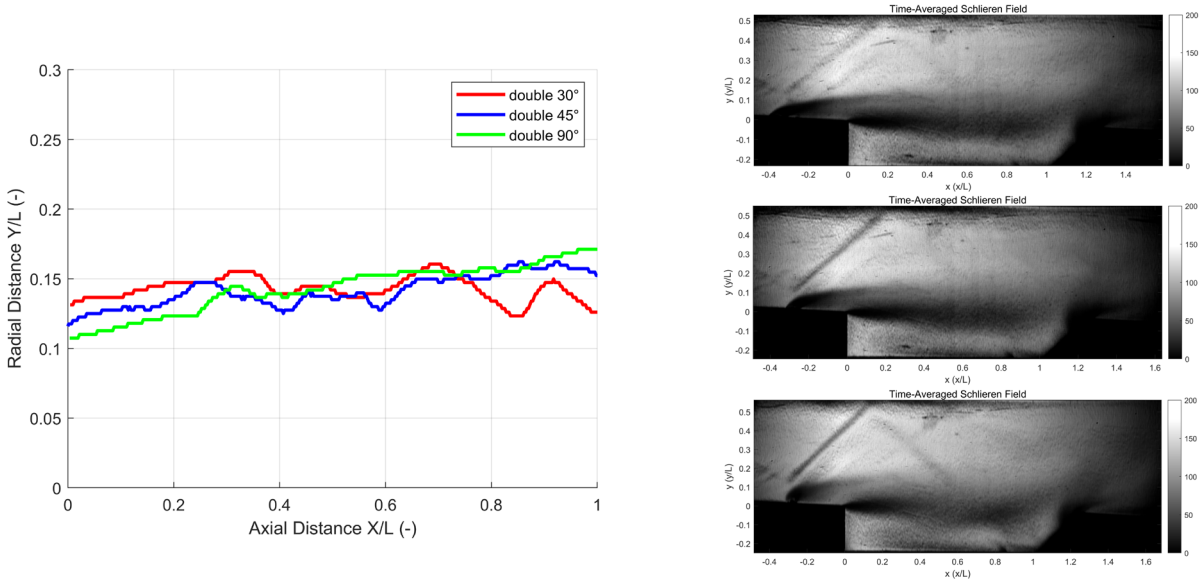
3.2.1. Jet Penetration Depth Under Reacting Flow Conditions

Quantitatively, combustion heat release increased the jet penetration depth for all three injection angles. The penetration evolution exhibited distinct two-stage characteristics due to the competition between the cavity shear layer lifting effect and the jet transverse momentum.

Near-field region ($x/L < 0.3$): The small-angle jet interacted more intensively with the cavity shear layer and was lifted rapidly by the large-scale vortical structures in the shear layer. Thus, the penetration depth showed an order of 30° > 45° > 90° in this region.

Mid-to-far field region ($x/L > 0.5$): The intrinsic transverse momentum of the jet became the dominant factor. The penetration depth returned to the classic order of 90° > 45° > 30°, which is consistent with the cold-flow trend at $x/L = 1$.

For the reacting flow, there was a great increase in penetration at the same axial position. For example, for the 90° injection, the penetration depth in the reacting flow field was 0.15 y/L at the axial position of $x/L = 0.4$. Compared with the cold-flow benchmarks, heat release increased the penetration depth in the front half of the cavity by about 25%, 22%, and 20% for the 30°, 45°, and 90° schemes, respectively. This kind of angle-dependent combustion-induced penetration augmentation decreased when the injection angle became steeper.



(**a**) (**b**)

Figure 3. Jet penetration depth characteristics and schlieren flow field structure in supersonic reacting flow: (**a**) variation in jet penetration depth in supersonic reacting flow, normalized by $L_{bottom} = 78.8$ mm; (**b**) time-averaged reacting flow schlieren flow fields at injection angles of 30°, 45° and 90° are arranged from top to bottom, demonstrating jet-induced shock structures and cavity shear layer characteristics.

We can attribute this tendency to the fact that, for the reacting flow, the interaction between the small-injection-angle jet and the cavity shear layer was more intensive; the thermal expansion from heat release further lifted the shear layer and amplified the penetration enhancement effect [13,16]. The curve crossover around $x/L \approx 0.3 - 0.5$ was a natural result of the transition between the two dominant mechanisms, which is a typical phenomenon in cavity-stabilized supersonic combustion with upstream injection.

3.2.2. Flow Structure Evolution in Reacting Flow

The combined analysis of the schlieren visualizations and the penetration data explained two effects of the combustion heat release on the supersonic flow field.

Shock Structure Attenuation

The primary mechanism for the attenuation of jet-induced shock waves is the incoming flow boundary layer separation driven by combustion. In all cases, the uniformly distributed combustion heat release also reduced the intensity of the jet-induced shock structures. The most significant reduction was observed for the 90° injection case: the sharp bow shock in the cold flow turned into a mild density gradient in the reacting flow field. By contrast, the attenuation effect was the least pronounced for the 30° injection case: the weak oblique shock is barely visible in the schlieren images. (First, combustion-induced BL separation smears the sharp density jump into a more gradual gradient, reducing schlieren contrast. Second, heat release increases mean background density, reducing the relative density gradient across the shock. Importantly, shock strength (pressure ratio) is not necessarily reduced).

Shear Layer and Recirculation Zone Evolution

Combustion heat release induced significant thickening and upward lifting of the cavity shear layer. Compared with the cold-flow baseline, the growth amplitude of shear layer thickness and lifting height under reacting conditions is notably higher for the 30°

inclined injection than that for the 90° normal injection. This phenomenon was attributed to the stronger coupling interaction between the jet and cavity flow under 30° injection, which achieved more sufficient fuel–air mixing within the shear layer region. The enhanced premixing further promoted higher local combustion heat release intensity here, which in turn drove a more dramatic thermal expansion and uplift of the cavity shear layer.

3.2.3. Flow Field Distribution near the Cavity Under Reacting Flow Conditions

The angle-dependent combustion-induced penetration augmentation, being more pronounced at small injection angles, could be attributed to the inherent differences in cold-flow jet characteristics. For the 30° injection, the low initial jet penetration depth and weak transverse momentum made the jet highly sensitive to the incoming flow separation induced by combustion heat release. This led to a substantial enhancement in jet penetration, while weakening the interaction between the jet and the cavity shear layer. By contrast, the 90° injection featured higher cold-flow penetration and a stronger effective momentum-flux ratio, thus exhibiting a milder response to combustion-induced flow separation, with a smaller increment in penetration depth and a slighter reduction in jet-cavity interaction.

3.3. Flame Structure and Stability

Figure 4 showed the flame dynamics of the dual-injector configuration at the baseline conditions ($Ma = 1.6$, $T_0 = 660$ K, $\phi = 0.2$) for the injection angles of 30°, 45°, and 90°. The upper row was the time-averaged CH* chemiluminescence intensity distributions, which was a well-known mark of the flame spatial heat release profile. The lower row is the normalized CH* RMS fluctuation maps that quantified the unsteady combustion dynamics and the flame stability. In all the maps, we normalized the maps to the same color scale to allow a direct quantitative cross-comparison for all the test cases.

3.3.1. Time-Averaged Flame Distribution Under Different Injection Angles

An examination of time-averaged heat release fields showed that the overall spatial distribution of the flame was jointly governed by jet transverse momentum and cavity shear layer interaction, rather than a simple monotonic dependence on the injection angle.

In the fully developed mainstream region, increasing the injection angle elevated the effective transverse momentum flux of the jet, enhanced deep penetration into the core flow, improved fuel–air mixing, and promoted earlier entrainment of unburned fuel into the cavity recirculation zone. This led to earlier auto-ignition, upstream migration of the primary heat release zone, wider flame radial spread, and higher peak heat release intensity [13,17].

Quantitatively, this was confirmed by the fact that the 90° normal injection produced the most upstream primary heat release zone, the widest radial flame coverage, and the strongest reaction intensity, with the heat release region closely coinciding with the high-strength cavity recirculation zone characterized in Section 3.1. On the contrary, the 30° inclined injection resulted in a significantly downstream-shifted heat release core, with insufficient radial mixing into the mainstream and the lowest overall heat release intensity. The 30° jet was more deeply involved in the cavity shear layer in the near field, but its weak transverse momentum prevented it from penetrating into the supersonic core flow, resulting in the overall downstream migration of the flame.

3.3.2. Flame Stability Characteristics and Comparison

The normalized RMS fluctuation intensity of the primary heat release zone followed the order: 45° inclined injection > 30° injection > 90° normal injection. According to a widely accepted criterion for supersonic combustion, flame stability is inversely proportional to the fluctuation intensity of the core heat release region [13,16,18].

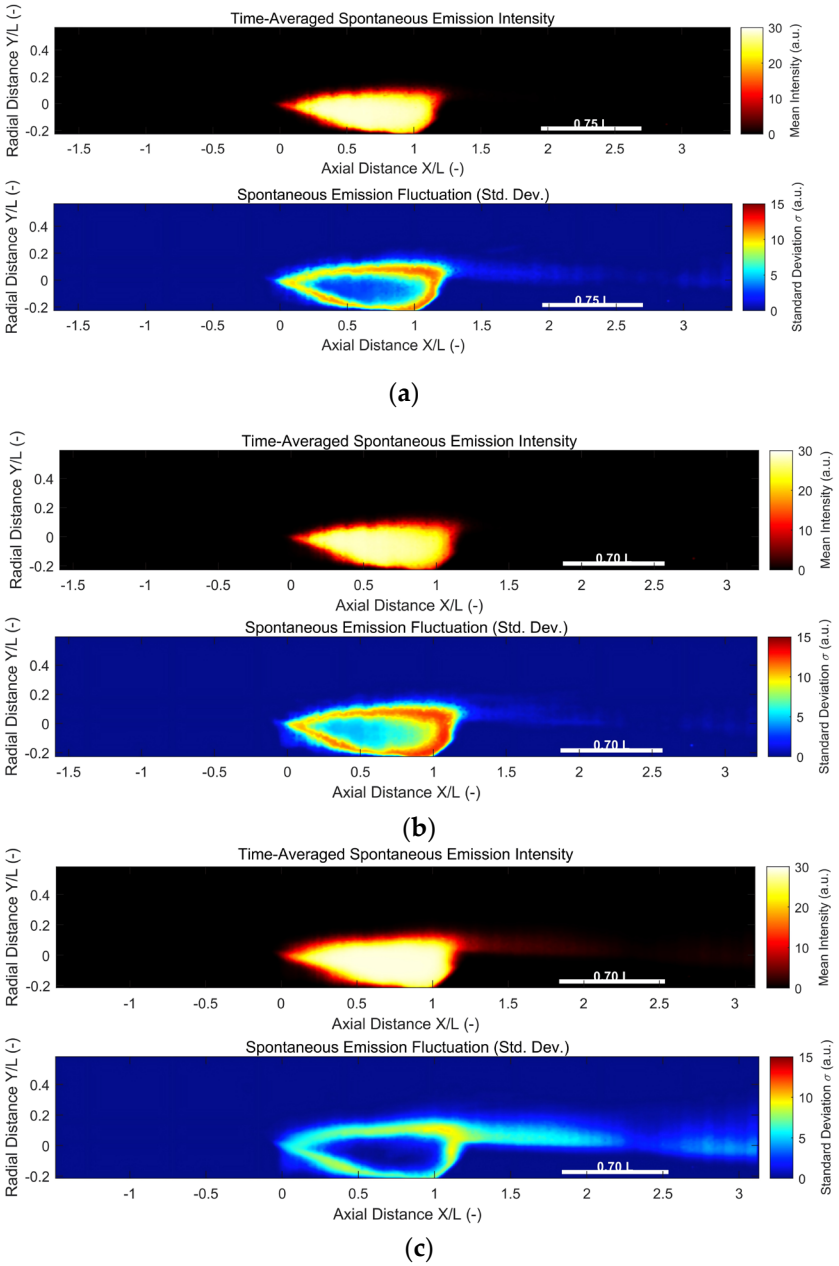


Figure 4. Mean and unsteady combustion characteristics of cavity flames with different dual-orifice injection angles by CH* chemiluminescence: (**a**) the injection angle is 30°; (**b**) the injection angle is 45°; (**c**) the injection angle is 90°. All the fluctuation intensities are normalized by the time-averaged intensity of the primary heat release zone for comparability.

For the 90° configuration, high-amplitude fluctuations only appeared at the trailing edge of the main heat release zone, and the peak normalized fluctuation intensity in the core combustion region is approximately 2 a.u. The flame core was anchored in the stable recirculation zone and isolated from freestream disturbances, thus achieving better flame stability.

For the 45° configuration, the flame front was fully aligned with the high-shear cavity shear layer, which drove the most intense unsteady fluctuations. The peak fluctuation intensity was much higher than that of the 90° baseline (about three times higher).

For the 30° configuration, the flame exhibited intermediate stability: high fluctuations are only distributed in the downstream periphery of the heat release core, with a peak intensity of approximately 4 a.u.—about twice that of the 90° case [16].

3.3.3. Overall Effects of Injection Angle on Combustion Performance

Consistent with the flow field evolution described in Sections 3.1 and 3.2, the observed flame fluctuation characteristics were directly governed by the spatial overlap between the flame front and the cavity shear layer.

For the 90° injection, the shear layer was elevated, and the flame was located in the stable part of the cavity recirculation zone, isolated from freestream disturbances, resulting in minimal fluctuation intensity.

For the 45° injection, the flame core was directly aligned with the high-shear shear layer, driving the most intense unsteady fluctuations.

For the 30° injection, the flame was located downstream of the main shear layer, with an intermediate fluctuation level.

It is worth noting that the 30° injection flame was mainly distributed within the cavity (including the shear layer), while for 45° and 90° injections, jet wake flames also existed in the mainstream flow in addition to the flame in the cavity shear layer. These jet wake flames extended further downstream of the cavity and exhibited strong oscillatory behavior.

This mechanism accounts for the non-monotonic stability tendency observed in the present dual-injector configuration. Whether a similar trend exists in single-injector or other multi-injector geometries requires further systematic investigation [19].

A combined analysis of jet penetration depth, flow structure, and flame characteristics defined two regimes of combustor performance response to injection angle:

Under cold-flow conditions, jet penetration exhibits a two-stage characteristic: the cavity shear layer lifting effect dominates in the near field, while jet transverse momentum dominates in the far field. The overall penetration capability and shock strength increase with injection angle in the fully developed region.

Under reacting conditions, flame stability presented a distinct non-monotonic trend, jointly determined by flame–shear layer overlap and heat release feedback. Specifically, as shown in Figure 4, the 45° injection configuration presents the strongest unsteady fluctuations, forming a non-monotonic flame unsteadiness characteristic different from the two-stage trend in cold flow.

4. Conclusions

The main findings of this work are summarized as follows.

Under cold-flow conditions (Section 3.1), the overall jet penetration capacity in the fully developed far field increased with injection angle following the order of 90° > 45° > 30°, as quantified in Figure 2a. A larger injection angle brought a faster fuel–air mixing rate and stronger jet-induced shock waves, accompanied by higher total pressure loss.

Combustion heat release significantly elevated the jet penetration depth for all injection angles (Section 3.2.1, Figure 3a). The relative penetration increment showed a strong angle dependence: the maximum increment (~25%) occurred at the 30° injection, and decreased gradually to ~20% at the 90° injection. As revealed in Section 3.2.3, combustion-induced inflow separation greatly boosts jet penetration while weakening the jet–cavity interaction, which accounts for the more pronounced enhancement at smaller injection angles.

The flame distribution and stability varied remarkably with injection angle (Section 3.3, Figure 4). The 30° injection flame is confined within the cavity, whereas the flame expands into the mainstream and forms evident jet wake flames at 45° and 90°. The flame stability follows the order of 90° > 30° > 45°. This non-monotonic stability trend is a characteristic feature of the tested dual-injector configuration under the present operating conditions, and its generalization to other injector configurations requires further study.

Author Contributions: Conceptualization, L.L. and J.L.; investigation, L.L.; writing—original draft, L.L.; writing—review & editing, J.L.; supervision, J.L. All authors have read and agreed to the published version of the manuscript. Doubao was used to check for textual errors and inappropriate expressions in the manuscript, and Grammarly was used for language proofreading.

Funding: This research received no external funding.

Data Availability Statement: The data presented in this study are available on request from the corresponding author due to the relevance of the datasets to ongoing unpublished research in the laboratory.

Conflicts of Interest: The authors declare no conflict of interest.

References

1. Luo, F.; Song, W.; Li, J.; Chen, W.; Long, Y. Experimental Study of Kerosene Supersonic Combustion with Pilot Hydrogen and Fuel Additive under Low Flight Mach Conditions. *Energy* **2021**, *222*, 119858. [CrossRef]
2. Li, X.; Lei, Q.; Zhao, X.; Fan, W.; Chen, S.; Chen, L.; Tian, Y.; Zhou, Q. Combustion Characteristics of a Supersonic Combustor with a Large Cavity Length-to-Depth Ratio. *Aerospace* **2022**, *9*, 214. [CrossRef]
3. Xiong, P.; Zheng, D.; Tan, Y.; Tian, Y.; Le, J. Experimental Study of Ignition and Combustion Characteristics of Ethylene in Cavity-Based Supersonic Combustor at Low Stagnation Temperature and Pressure. *Aerosp. Sci. Technol.* **2021**, *109*, 106414. [CrossRef]
4. Relangi, N.; Ingenito, A.; Jeyakumar, S. The Implication of Injection Locations in an Axisymmetric Cavity-Based Scramjet Combustor. *Energies* **2021**, *14*, 2626. [CrossRef]
5. Wang, K.; Cao, W. Numerical Investigation of Mixing Enhancement in a Cavity-Based Supersonic Combustor Using the Upstream Wavy Wall. *Int. J. Hydrogen Energy* **2025**, *114*, 18–30. [CrossRef]
6. Gruber, M.R.; Nejad, A.S.; Chen, T.H.; Dutton, J.C. Mixing and Penetration Studies of Sonic Jets in a Mach 2 Freestream. *J. Propuls. Power* **1995**, *11*, 315–323. [CrossRef]
7. Portz, R.; Segal, C. Penetration of Gaseous Jets in Supersonic Flows. *AIAA J.* **2006**, *44*, 2426–2429. [CrossRef]
8. Gruber, M.R.; Baurle, R.A.; Mathur, T.; Hsu, K.-Y. Fundamental Studies of Cavity-Based Flameholder Concepts for Supersonic Combustors. *J. Propuls. Power* **2001**, *17*, 146–153. [CrossRef] [PubMed]
9. Ben-Yakar, A.; Hanson, R.K. Cavity Flame-Holders for Ignition and Flame Stabilization in Scramjets: An Overview. *J. Propuls. Power* **2001**, *17*, 869–877. [CrossRef] [PubMed]
10. Rothstein, A.; Wantuck, P. A Study of the Normal Injection of Hydrogen into a Heated Supersonicflow Using Planar Laser-Induced Fluorescence. In Proceedings of the 28th Joint Propulsion Conference and Exhibit, Nashville, TN, USA, 6–8 July 1992. [CrossRef]
11. Ogawa, H. Effects of Injection Angle and Pressure on Mixing Performance of Fuel Injection via Various Geometries for Upstream-Fuel-Injected Scramjets. *Acta Astronaut.* **2016**, *128*, 485–498. [CrossRef]
12. Ji, J.; Cai, Z.; Wang, T.; Wang, Z.; Sun, M. Experimental Study on Combustion Modes and Oscillations in a Cavity-Based Scramjet Combustor. *AIAA J.* **2024**, *62*, 915–927. [CrossRef]
13. Yuan, Y.; Zhang, T.; Yao, W.; Fan, X. Study on Flame Stabilization in a Dual-Mode Combustor Using Optical Measurements. *J. Propuls. Power* **2015**, *31*, 1524–1531. [CrossRef]
14. Guardone, A.; Zocca, M.; Gajoni, P.; Mondonico, F.; Conti, C.C. Characteristics-Based Measurements of Supersonic Flows from Schlieren Images. *Exp. Fluids* **2025**, *66*, 72. [CrossRef]
15. Dai, J.; Chen, L.; Kong, F. Research on the Mixing Characteristics of a Cavity Based Supersonic Combustion Chamber Coupled with Secondary Recirculation Jets. *Int. J. Hydrogen Energy* **2024**, *92*, 516–526. [CrossRef]
16. Meng, Y.; Sun, W.; Gu, H.; Chen, F.; Zhou, R. Supersonic Combustion Mode Analysis of a Cavity Based Scramjet. *Aerospace* **2022**, *9*, 826. [CrossRef]
17. Zhao, Y.; Tian, Y.; Du, G.; Zhou, Y. Research on the Influence of Cavity Ramp Angle on Combustion Oscillation Process in Scramjet Combustor. *Appl. Therm. Eng.* **2025**, *279*, 127561. [CrossRef]
18. Mahesh, S.; Mishra, D.P. Dynamic Sensing of Blowout in Turbulent CNG Inverse Jet Flame. *Combust. Flame* **2015**, *162*, 3046–3052. [CrossRef]
19. Micka, D.J.; Driscoll, J.F. Combustion Characteristics of a Dual-Mode Scramjet Combustor with Cavity Flameholder. *Proc. Combust. Inst.* **2009**, *32*, 2397–2404. [CrossRef]

Disclaimer/Publisher's Note: The statements, opinions and data contained in all publications are solely those of the individual author(s) and contributor(s) and not of MDPI and/or the editor(s). MDPI and/or the editor(s) disclaim responsibility for any injury to people or property resulting from any ideas, methods, instructions or products referred to in the content.